ACS OMEGA

http://pubs.acs.org/journal/acsodf

Article

Corrosion Inhibition of Azo Compounds Derived from Schiff Bases on Mild Steel (XC70) in (HCl, 1 M DMSO) Medium: An Experimental and Theoretical Study

Ammar Zobeidi, Salah Neghmouche Nacer, Salem Atia, Latifa Kribaa, Aicha Kerassa, Abasse Kamarchou, Mousa AlNoaimi, Djamel Ghernaout, Mohamed A. Ali, Abdelmajeed Adam Lagum, and Noureddine Elboughdiri*

Cite This: *ACS Omega* 2023, 8, 21571−21584

Read Online

ACCESS | Metrics & More | Article Recommendations

ABSTRACT: The inhibitory activity of three prepared azo compounds derived from Schiff bases, namely, bis[5-(phenylazo)-2-hydroxybenzaldehyde]-4,4′-diaminophenylmethane (C1), bis[5-(4-methylphenylazo)-2-hydroxybenzaldehyde]-4,4′-diaminophenylmethane (C2), and bis[5-(4-bromophenylazo)-2-hydroxybenzaldehyde]-4,4′-diaminophenylmethane (C3), against corrosion of steel type XC70 in (HCl, 1 M DMSO) medium was investigated experimentally by electrochemical measurements and theoretically using density functional theory (DFT). The correlation between corrosion inhibition and concentration is direct. The maximum inhibition efficiency at 6×10^{-5} M for the three azo compounds derived from Schiff bases was 64.37, 87.27, and 55.47% for C1, C2, and C3, respectively. The Tafel curves indicate that the inhibitors follow a mixed but predominantly anodic inhibitor system and have a Langmuir isothermal adsorption process. The observed inhibitory behavior of compounds was supported by DFT calculation. It was also found that there was a strong correspondence between the theoretical and experimental results.

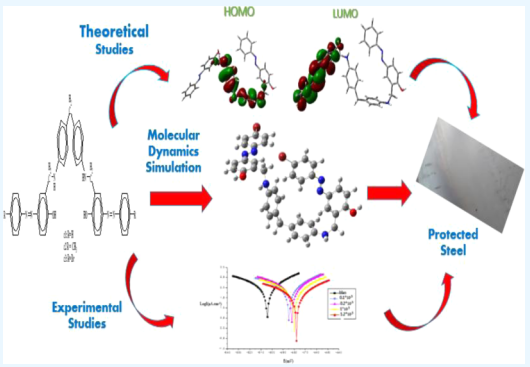

1. INTRODUCTION

Organic inhibitors are among the most critical methods for inhibiting corrosion in acidic environments.[1,2] Acid solutions are used in many industrial processes, and organic inhibitors protect several minerals against acid.[3,4] Compounds containing heteroatoms (N, P, S) have proven a good inhibitor efficiency. Indeed, several heterocyclic compounds are corrosion protection inhibitors with high performance in acidic medium. Furthermore, these organic molecules can be adsorbed on the surface of the metal, which lowers the corrosion rate in an acidic environment.[5−7]

Schiff bases and their derivatives have recently become widely used as corrosion inhibitors thanks to their low cost and good inhibiting effect.[8−13] Corrosion inhibitors mainly depend on the adsorption phenomenon and how they inhibit corrosion. The presence of double bonds and heterogeneous atoms such as sulfur, phosphorus, nitrogen, and oxygen make these compounds suitable inhibitors.[14−17]

In this work, three azo compounds derived from Schiff bases, namely, bis[5-(phenylazo)-2-hydroxybenzaldehyde]-4, 4′-diaminophenylmethane (C1), bis[5-(4-methylphenylazo)-2-hydroxybenzaldehyde]-4,4′-diaminophenylmethane (C2), and bis[5-(4-bromophenylazo)-2-hydroxybenzaldehyde]-4,4′-diaminophenylmethane (C3) (Figure 1), were prepared. An investigation was carried out using electrochemical methods to

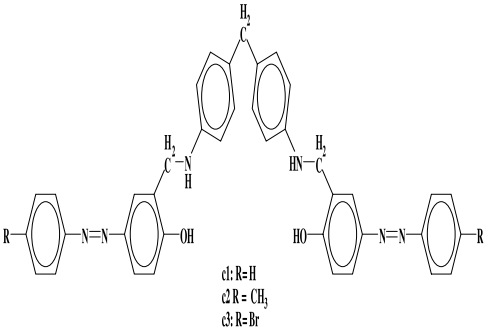

Figure 1. Structure of the studied inhibitors (C1, C2, and C3).

Received: February 4, 2023
Accepted: May 24, 2023
Published: June 5, 2023

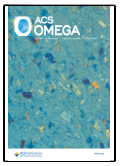

https://doi.org/10.1021/acsomega.3c00741
ACS Omega 2023, 8, 21571−21584

Table 1. Physical and Elemental Analysis Data of the C1, C2, and C3 Schiff Bases

compound	compound formula	formula weight (g mol^{-1})	yield (%)	color	$\lambda_{max\ in\ DMF\ (nm)}$	found (calculated) %C	%H	%N
C1	$C_{39}H_{34}O_2N_6$	618.62	88.44	yellow	385	75.71 (75.45)	5.54 (5.83)	13.58 (13.35)
C2	$C_{41}H_{38}O_2N_6$	646.67	75.89	light brown	360	76.14 (75.76)	5.92 (5.95)	12.99 (13.13)
C3	$C_{39}H_{32}O_2N_6Br_2$	776.42	69.20	sepia	363	60.32 (59.83)	4.15 (4.04)	10.82 (10.97)

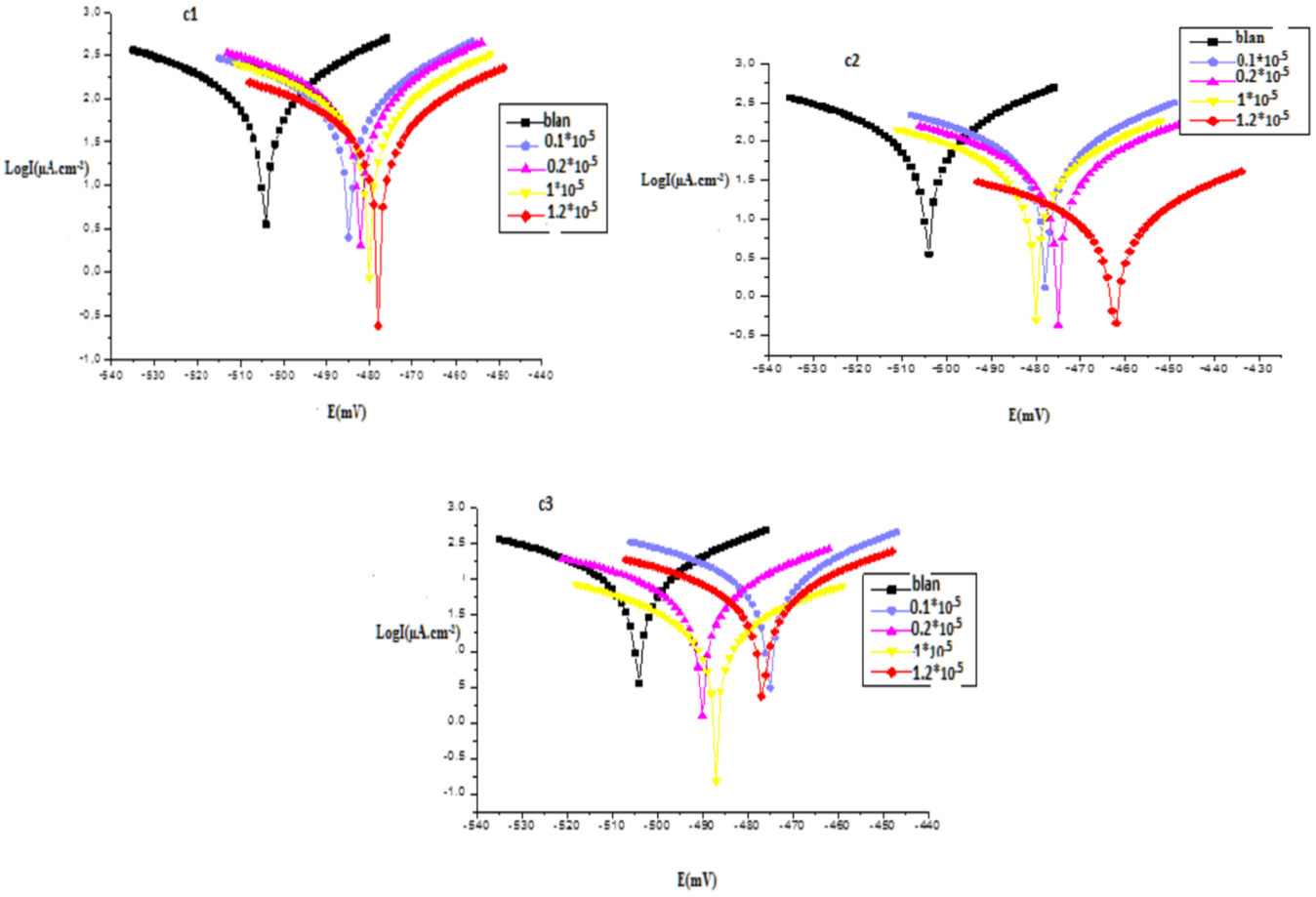

Figure 2. Tafel polarization curves of three inhibitors (C1, C2, and C3) at 25 °C.

determine the influence of the donating groups of these azo compounds (bromo and methyl) on the corrosion inhibition provided towards iron (HCl, 1 M DMSO). Calculations based on density functional theory (DFT) were utilized to explain the action mechanism of the inhibitors, besides their electrical characteristics and structural influences on how effectively they inhibit.

In addition, the circumstances that led to the production of two different ZnO deposits on an indium tin oxide substrate were investigated. These conditions changed the proportions of zinc oxide salt. The initial deposits were acquired from an aqueous mixed bath containing the salt at a lower concentration and temperature. Meanwhile, the second deposits were produced by annealing simonkolleite ($Zn_5(OH)_8Cl_2H_2O$) for 1 h at 400 °C. In addition, the changes in structural and morphological analytical results for both deposits were compared to those of the simonkolleite phase. These discrepancies were observed in both deposits. Impedance spectroscopic curves and the photoelectrochemical behavior of three films are also explored in this study. This research provides information on the electrical conductivity of the deposits as well as their photosensitivity.

2. EXPERIMENTAL SECTION

2.1. Solution and Specimen Preparation. The chemicals utilized in the current study were obtained from Merck and were of reagent-grade quality. Three azo compounds, C1, C2, and C3, were synthesized using published methods.[18,19] The physical and analytical data for the Schiff bases are given in Table 1. The structures of the synthesized Schiff bases were identified using spectroscopic techniques such as IR, UV−vis, ^{1}H NMR, and ^{13}C NMR. The Schiff base derivatives used in this study are presented in Figure 1.

The considered mild steel (XC70) is commercially available in the following composition (wt %): 0,065% C; 0.01% S; 0.245% Si; 1.685% Mn; 0.002% P; 0.042% Cr; 0.062% N; 0.010% Cu; 0.042% Al; 0.067% Nb; 0.014% V; 0.019% Ti; 0.005% Mo; and the rest is Fe. The steel was cut into cylindrical disks and was the working electrode in all electrochemical studies. The acidic medium (HCl, 1 M) was prepared from distilled water and HCl of 37% purity. The azo compounds

https://doi.org/10.1021/acsomega.3c00741
ACS Omega 2023, 8, 21571−21584

Table 2. Electrochemical Parameters Determined by the Tafel Method of the Inhibitors (C1, C2, and C3) at 25 °C

compounds	C_{inh} (M)	$-E_{corr}$ (mV/SCE)	β_a (mV/dec)	$-\beta_c$ (mV/dec)	i_{corr} (μA/cm^2)	IE$_p$ (%)
C1	blank	504.3	82.5	53.6	101.80	
	1×10^{-6}	484.7	46.5	35.8	75.97	25.37
	2×10^{-6}	480.2	40.3	33.2	72.28	28.99
	1×10^{-5}	480.1	37.5	31.6	49.61	51.26
	6×10^{-5}	477.9	43.2	33.6	35.95	64.37
	SD	253.41	27.00	17.67	31.75	25.31
	Pearson χ^2	−0.72	0.11	−0.10	−0.87	0.87
C2	blank	504.3	44	55	101.80	
	1×10^{-6}	477.8	47.6	41.6	52.41	48.51
	2×10^{-6}	475.1	37.8	31.9	38.43	62.21
	1×10^{-5}	480.1	83.4	55.2	28.39	72.11
	6×10^{-5}	462.4	44	55	12.95	87.27
	SD	251.19	27.09	23.21	30.78	26.28
	Pearson χ^2	−0.93	−0.17	0.63	−0.87	0.87
C3	blank	504.3	49.9	39.8	101.80	
	1×10^{-6}	475.2	50.9	89.39	84.18	17.37
	2×10^{-6}	490.2	98.5	83.5	53.64	47.37
	1×10^{-5}	487	45	36.9	46.75	54.07
	6×10^{-5}	476.5	49.9	39.8	45.40	55.47
	SD	254.91	30.83	30.36	32.54	17.36
	Pearson χ^2	−0.45	−0.36	−0.65	−0.53	0.53

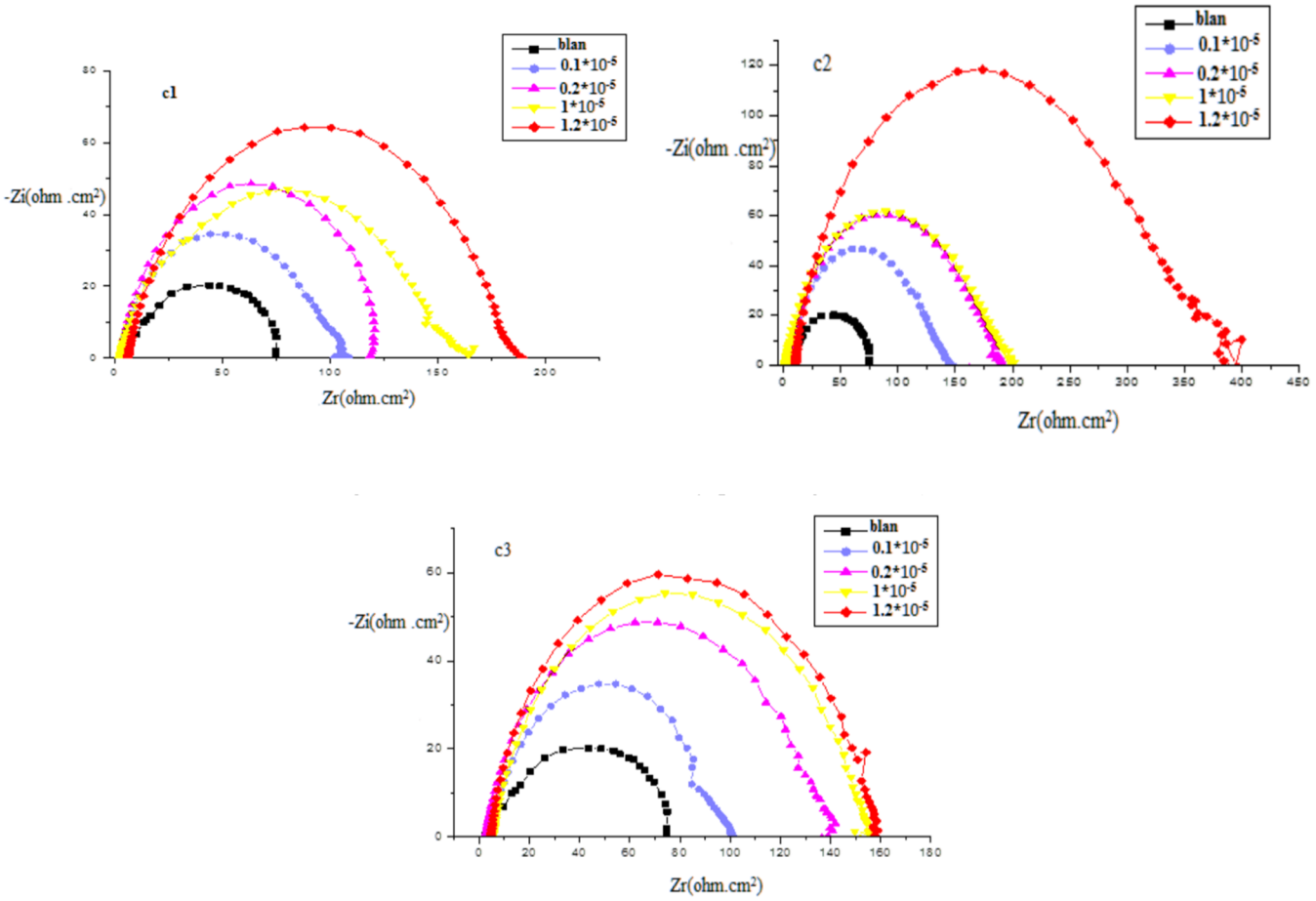

Figure 3. Mild steel corrosion Nyquist diagrams in (HCl, 1 M DMSO) media at 25 °C without and with different concentrations of three inhibitors (C1, C2, and C3).

(inhibitors) were dissolved in DMSO, so the corrosive medium was (HCl, 1 M DMSO). The concentrations of C1, C2, and C3 used as inhibitors ranged from 10^{-6} to 6×10^{-5} M.

2.2. Measurements Using Electrochemistry. The electrochemical investigation was carried out with the assistance of a Voltalab40 (PGZ301) equipped with a Volta-master4 type

https://doi.org/10.1021/acsomega.3c00741
ACS Omega 2023, 8, 21571−21584

Table 3. Impedance Parameters for Corrosion of Mild Steel (XC70) in (HCl, 1 M DMSO) without and with Different Concentrations of the Inhibitors (C1, C2, and C3) at 25 °C

compounds	C_{inh} (M)	R_{ct} (Ω cm^2)	C_{dl} (μF/cm^2)	n	IE (%)	θ
C1	blank	73	153.5	0.8772		
	1×10^{-6}	103.3	61.77	0.7281	29.33	0.2933
	2×10^{-6}	111.4	65.29	0.7591	34.47	0.3447
	1×10^{-5}	147.8	70.79	0.7761	50.60	0.5060
	6×10^{-5}	186.7	54.14	0.7884	61.78	0.6178
	SD	43.83	40.92	0.055	23.55	0.24
	Pearson χ^2	0.93	−0.76	1.00	0.87	0.87
C2	blank	73	153.5	0.8762		
	1×10^{-6}	97.98	57.88	0.7781	48.32	0.4832
	2×10^{-6}	185.1	67.16	0.7876	60.5	0.605
	1×10^{-5}	195	81.54	0.7894	62.56	0.6256
	6×10^{-5}	371.4	84.03	0.7937	80.18	0.8018
	SD	117.22	37.70	0.040	30.34	0.30
	Pearson χ^2	0.95	0.72	1.00	0.92	0.92
C3	blank	73	153.5	0.8736		
	1×10^{-6}	97.98	66.66	0.7491	25.49	0.2549
	2×10^{-6}	138.8	101.9	0.7631	47.40	0.4740
	1×10^{-5}	151	86.46	0.7781	51.56	0.5156
	6×10^{-5}	154.4	42.03	0.7957	52.72	0.5272
	SD	35.87	41.93	0.048	22.67	0.23
	Pearson χ^2	0.57	−0.81	1.00	0.53	0.53

program and a 500 mL cylindrical glass cell with five holes (one for the XC70 metal working electrode (WE), the second for the platinum wire auxiliary electrode, and the third for the reference electrode (RE), i.e., saturated calomel electrode (SCE)). The WE was scraped before the start of each test with emery paper (80, 200, 1200, and 4000), then washed with distilled water and acetone, and finally well dried. Cathode and anode branches were acquired in the field −600 to −250 mV/ECS at a 30 mV/sec scan rate. The corrosion potential (E_{corr}) and current density (i_{corr}) were determined by extrapolating data from Tafel curves. The inhibition efficiency (IE_p, in %) was determined using eq 1[20]

$$IE_p\ (\%) = \frac{i_{corr} - i_{corr(inh)}}{i_{corr}} \times 100 \quad (1)$$

where $i_{corr(inh)}$ and i_{corr} are the corrosion current densities with an inhibitor and without an inhibitor, respectively.

Electrochemical impedance spectroscopy (EIS) studies were all done at 25 °C. The inhibition efficiency (IE_{EIS}, in %) was determined using eq 2[21]

$$IE_{EIS}\ (\%) = \frac{R_{t,inh} - R_{t,corr}}{R_{t,inh}} \times 100 \quad (2)$$

where $R_{t,inh}$ and $R_{t,corr}$ are the charge transfer resistances with and without an inhibitor, respectively.

2.3. Computational Details. DFT calculations were based on B3LYP,[22] which is functional with 6-311G(d,p) and 6-31G(d,p) basis sets,[23] and implemented in GAUSSIAN 09 software.[24−28] On an Intel Core i3-3120M laptop with 2.50 GHz and 6.00 Go RAM, frequency analysis was used to ensure that the optimized geometry was not a saddle point.

3. RESULTS AND DISCUSSION

3.1. Tafel Curves. Figure 2 shows the Tafel curves of steel (XC70) in the solution consisting of HCl and 1 M DMSO, both with and without the presence of inhibitors of varying concentrations. Table 2 lists the electrochemical properties of i_{corr} and E_{corr} vs SCE, anodic and cathodic Tafel slopes (b_a, b_c), and IE. Electrochemical polarization measurements show that both cathodic and anodic current densities decreased with increasing inhibitor concentrations. This indicates that inhibitors reduce both the cathodic reduction reaction (eq 3) and metal dissolution (eq 4).

In addition, increasing the inhibitor concentration slightly modifies the cathodic slope, indicating that the cathodic reaction mechanism has not been altered. The presence of inhibitors changes the corrosion potential toward the nobler potential compared to the result obtained without inhibitors. In contrast, the maximum change in E_{corr} values was −41.9 mV, less than ±85 mV. This indicates that these inhibitors act as a mixed type, even if the anodic inhibition is predominant.[29−31] Furthermore, the inhibitory activity increased with increasing inhibitor concentration and reached values of 64.37, 87.27, and 55.47% for C1, C2, and C3, respectively, at the optimum concentration (6×10^{-5} M).

As illustrated by such findings, the inhibitory activity of C2 is greater than that of other azo compounds. Indeed, the methyl group ($-CH_3$), which has an inducing donor effect, makes the inhibitors form a stronger coordination bond with iron than the electron withdrawing bromine (−Br) group.[32]

$$2H^+ + 2e^- \rightarrow H_{2(g)} \quad (3)$$

$$Fe - 2e^- \rightarrow Fe^{2+} \quad (4)$$

3.2. Impedance. A standard Randle's circuit obtained from a capacitive semicircle in impedance spectra for cases of corrosion of steels in an acidic medium has been described in the literature.[33,34] The Nyquist plots for iron in the (HCl, 1 M DMSO) solution are shown in Figure 3, both without any inhibitors and with a range of different concentrations of C1, C2, and C3 inhibitors. The impedance plots exhibit a nonideal semicircle in the presence and absence of an inhibitor. This is probably due to the mild steel's surface heterogeneity, which is

https://doi.org/10.1021/acsomega.3c00741
ACS Omega 2023, 8, 21571−21584

usually attributed to frequency dispersion and surface homogeneity. The deviation is explained by the roughness and impurities resulting from the formation of porous layers of inhibitors on the surfaces.[35,36] The diameter of the capacitive ring is directly proportional to the concentration due to the inhibitors' adsorption on the metal surface. This adsorption results from the interaction between the inhibitors' nitrogen and oxygen and the steel's character, which allows forming a film on the surface. The aromatic system can also contribute as π-electrons enhance the absorption of inhibitors on the surface and increase their efficiency.[37,38] An increase in absolute impedance at lower frequencies, generally shown by Bode plots, results in more excellent protection at greater inhibitor concentrations. The observation of a single-phase peak in the center frequency range indicates only one stable contact of the electric double layer, as shown in Figure 3.

Table 3 lists the electrochemical parameters such as pseudo-capacitance (C_{dl}), transfer resistance (R_{ct}), and IE that have been calculated for different concentrations of inhibitors C1, C2, and C3 in the medium (HCl, 1 M DMSO) for XC70 steel type.

On the one hand, R_{ct} values have been calculated at higher and lower frequencies from the differences in impedance. On the other hand, C_{dl} values were obtained at $f_{(-zi_{max})}$ frequency, at which the imaginary component of the impedance is maximal, using eq 3[39,40]

$$C_{dl} = \frac{1}{2\pi f_{(-zi_{max})}} \times \frac{1}{R_{ct}} \quad (5)$$

where C_{dl} is the pseudo-capacitance, R_{ct} is the transfer resistance, and $f_{(-zi_{max})}$ is the maximal frequency.

Also, the R_{ct} of the double-layer decreased (C_{dl}) and IE increased with increasing inhibitor C1, C2, and C3 concentrations. By increasing the interactions, the number of inhibitors adsorbed on the metal surface increased, reducing the number of active sites exposed to corrosion.[40] The inhibitor (C2) was found to have the highest percentage of inhibition efficiency (80.18%) compared to C1 (61.78%) and C3 (52.72%).

On the other hand, the variation in phase shift values (n) is not significant, thus confirming that the mechanism of dissolution of XC70 in HCl, 1 M DMSO in both the absence and presence of inhibitors is controlled by charge transfer. Moreover, in the presence of inhibitors C1, C2, and C3, n is found to be between 0.72 and 0.79, and these values are lower than those obtained in a blank solution (0.87). This is due to an increase in surface inhomogeneity as a result of inhibitor adsorption.[20]

The equivalent electrical circuit represents the mild steel/solution interface in the absence and presence of the inhibitor (Figure 4). The circuit consists of the electrolytic resistance (R_s), the charge transfer resistance (R_{ct}), and the constant phase element (CPE). The CPE parameter replaces the double-layer capacitance (C_{dl}) to fit the experimental results better.39 It is recommended to use the CPE instead of the pure capacitor to model the frequency dispersion, generally related to surface heterogeneity caused by corrosion in an acidic medium.

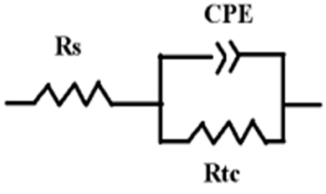

Figure 4. Electrochemical equivalent circuit used for simulating the impedance spectra.

3.3. Adsorption Study. An adsorption isotherm is required to investigate corrosion in the presence of organic chemicals to determine their inhibitory mechanism. The Langmuir, Timken, and Franken isotherms[40−42] have been utilized.

$$\frac{C_{inh}}{\theta} = \frac{1}{K_{ads}} + C_{inh} \quad \text{(Langmuir isotherm)} \quad (6)$$

$$e^{f\theta} = K_{ads} \quad \text{(Timken isotherm)} \quad (7)$$

$$\frac{\theta}{1-\theta} e^{2a\theta} = K_{ads} C_{inh} \quad \text{(Franken isotherm)} \quad (8)$$

where C_{inh} is the inhibitor concentration, Θ is the surface coverage, and K_{ads} is the adsorption balance constant.

The inhibitors' adsorption on the steel surface can explain the corrosion inhibition mechanism by preparing organic azo compounds. There are two types of adsorption, namely, chemical and physical. The first occurs on the (lone pair) inhibitor (d orbital) coordination bond. To investigate which isotherms are best suited for adsorption, Franken, Langmuir, and Temkin isotherms were tested, and the obtained results are presented in Table 4 and Figure 5. The linear correlation value closest to unity was obtained with the Langmuir isotherm, and the value of the slope of this isotherm is close to unity. This means that the adsorption process on the metal surface of the compound (C1, C2, and C3) follows the Langmuir isotherm.[42] From the Langmuir isotherm (eq 6), the adsorption constant (K_{ads}, ΔG°_{ads}) can be calculated using eqs 9 and 10, respectively[41]

Table 4. Linear Correlation of the Different Adsorption Isotherms of Inhibitors (C1, C2, and C3) on Mild Steel (XC70) in (HCl, 1 M DMSO) at 25 °C

compounds	Langmuir	Franken	Temkin
C1	0.998	0.923	0.854
C2	0.999	0.901	0.944
C3	0.999	0.182	0.679

$$K_{ads} = \frac{1}{55.5} e^{-(\Delta G^{\circ}_{ads}/RT)} \quad (9)$$

$$\Delta G^{\circ}_{ads} = -RT \ln(55.5 K_{ads}) \quad (10)$$

Table 5 presents the free enthalpy (ΔG°_{ads}) values of −42.58, −43.29, and −40.92 kJ/mol for azo compounds C1, C2, and C3, respectively. Again, the inhibitors' spontaneous adsorption onto the metal's surface was observed. The high values for the equilibrium constant of adsorption are a consequence of the powerful adsorption of C1, C2, and C3 on the surface of the mild steel (XC70) used in the experiment (HCl, 1 M DMSO).[43]

For the three inhibitors, ΔG° values were more significant than −40 kJ/mol, suggesting chemical adsorption.[44] Moreover, the absolute value of standard free energy (ΔG°) decreases in the following order: C2 > C1 > C3. Hence, the corrosion inhibition efficacy rises with increasing negative values (ΔG°_{ads}). This result agrees with the damping efficiency values obtained from impedance and Tafel polarization curves.

3.4. Scanning Electron Microscopy. Figure 6 shows micrographs of mild steel under pre- and post-immersion

https://doi.org/10.1021/acsomega.3c00741
ACS Omega 2023, 8, 21571−21584

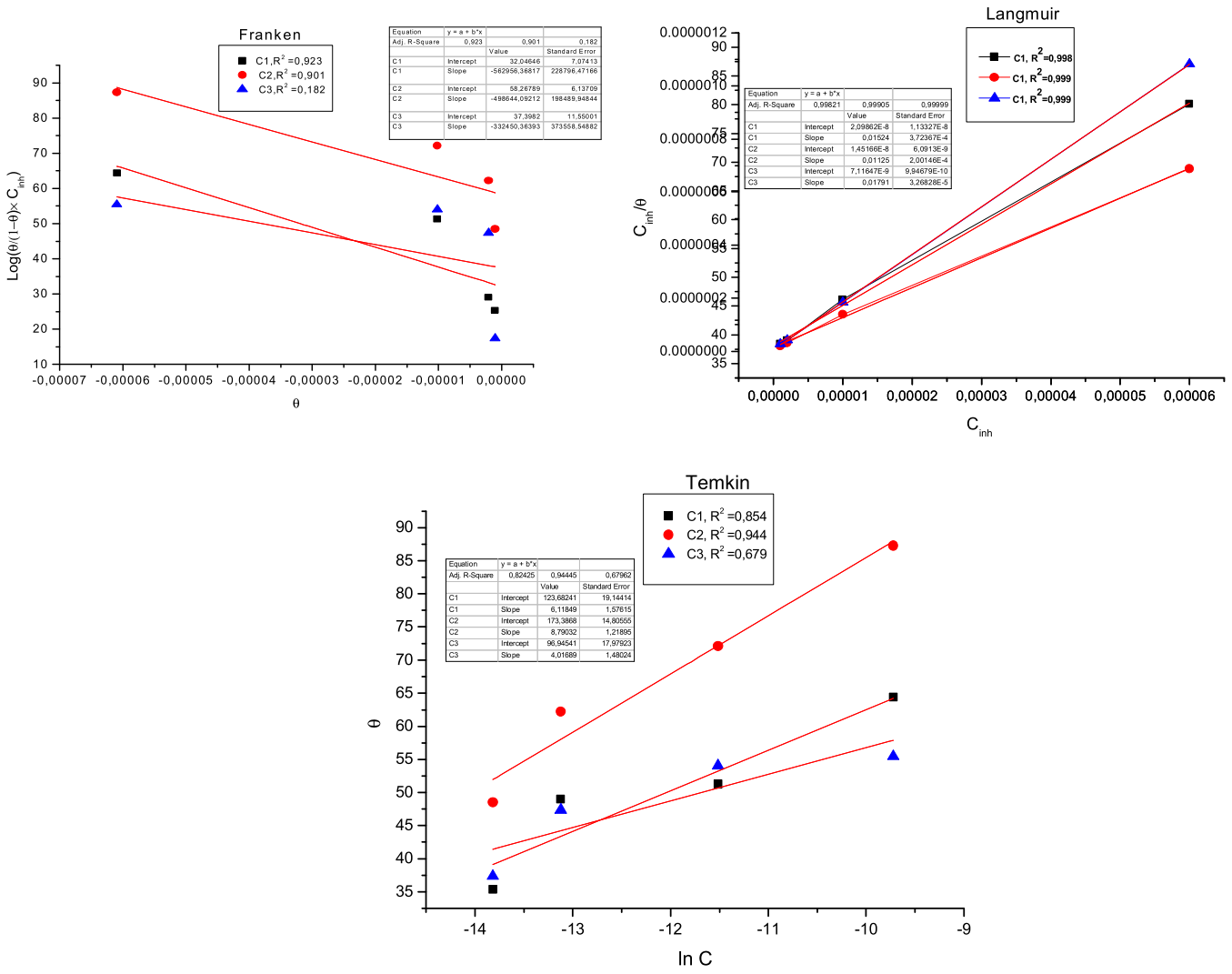

Figure 5. Different adsorption isotherms of inhibitors (C1, C2, and C3) on the mild steel surface in (HCl, 1 M DMSO) media at 25 °C.

Table 5. Linear Correlation of the Langmuir Isotherm and Thermodynamic Parameters of Adsorption of Inhibitors (C1, C2, and C3) on Mild Steel (XC70) in (HCl, 1 M DMSO) at 25 °C

compounds	C_{inh} (M)	$K_{ads} \times 10^5$ (M^{-1})	K_L	R^2	θ	$-\Delta G^{\circ}_{ads}$ (kJ/mol)
C1	1×10^{-6}	5.288207	0.6541	0.9990	25.37 ± 18.53	42.58
	2×10^{-6}		0.4859		28.99 ± 18.53	
	1×10^{-5}		0.1590		51.26 ± 18.53	
	6×10^{-5}		0.1361		64.37 ± 18.53	
C2	1×10^{-6}	7.062146	0.5860	0.9994	48.51 ± 16.33	43.29
	2×10^{-6}		0.4145		62.21 ± 16.33	
	1×10^{-5}		0.1240		72.11	
	6×10^{-5}		0.1055		87.27	
C3	1×10^{-6}	2.712232	0.7866	0.9995	17.37	40.92
	2×10^{-6}		0.6483		47.37	
	1×10^{-5}		0.2693		54.07	
	6×10^{-5}		0.2350		55.47	

conditions, where the immersion period was assumed to be 24 h at 25 °C in the absence and presence of inhibitors (C1, C2, and C3). Figure 6 demonstrates that in the absence of an inhibitor, the surface of mild steel is rougher and more porous due to the dissolution of mild steel (XC70) in (HCl, 1 M DMSO) medium. However, in the presence of inhibitors (C1, C2, and C3), the surface looks smooth, and practically all cavities have disappeared.

3.5. Contact Angle Measurement. Figure 7a–d shows the contact angle measurements in the absence (a) and the presence of the inhibitors C1 (b), C2 (c), and C3 (d). It can be seen that the angle in the absence of the inhibitor is smaller than that in its presence, indicating the occurrence of spacing between the

https://doi.org/10.1021/acsomega.3c00741
ACS Omega 2023, 8, 21571−21584

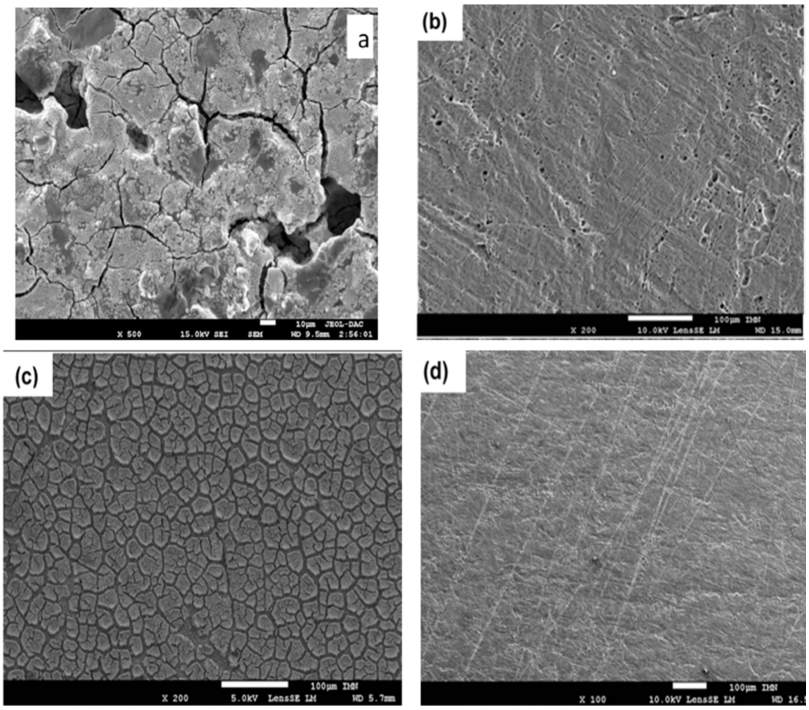

Figure 6. Surface morphology of the mild steel samples before and after immersion in uninhibited and inhibited (HCl, 1 M DMSO) at 25 °C: (a) free, (b) with inhibitor C1, (c) with inhibitor C2, and (d) with inhibitor C3 over 24 h.

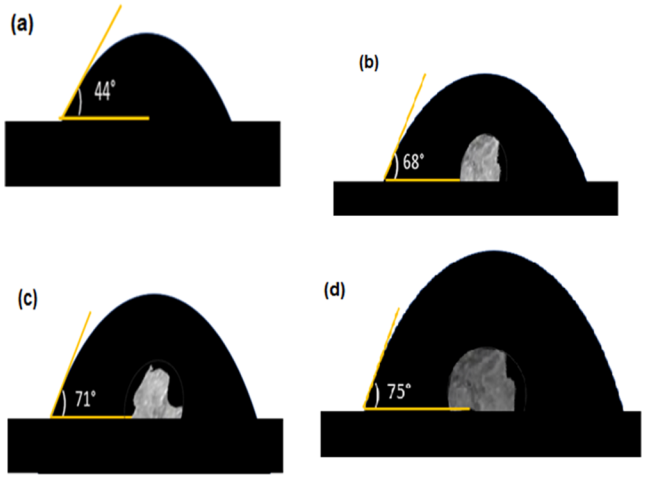

Figure 7. Measurement of the contact angle of a mild steel surface after a 24 h immersion in blank (a) and (HCl, 1 M DMSO) loaded with 10^{-5} M of three inhibitors C1 (b), C2 (c), and C3 (d).

water and the metal surface in the presence of the inhibitors C1, C2, and C3. On the other hand, the contact angle increased with increasing molecular weight and reached values of 68°, 71°, and 75° for C1, C2, and C3, respectively. This is because a larger molecular weight inhibitor has a greater tendency to remain as discrete droplets on the surface rather than spreading out, which results in a higher contact angle.[45] All of this proves that the inhibitors C1, C2, and C3 were adsorbed on the surface of mild steel.[20]

3.6. Density Functional Theory (DFT) Calculations. *3.6.1. Molecular Structure.* Bond lengths and angles for the studied three inhibitors are listed in Table 6 and shown in Figure 8. Also, Figure 9 shows that the studied molecules consist of two symmetrical parts. Indeed, the symmetry groups of all azo compounds are C1, and all dihedral angles in the selected moieties are equal to 0° or 180° due to the resonance effect, supporting the inhibitors' planarity. Electrons may be, however, exchanged between inhibitors' atoms and functional groups with the electrode surface. This phenomenon is influenced by structural and electronic properties such as chain length, molecule planarity, molecular volume, availability of the lone pair of electrons that are present on the heteroatoms (O, N, and S), polarity, dipole moment, the energy of frontier molecular orbitals, and instauration or aromatic ring, are generally considered to be effective corrosion inhibitors.[46,47]

Table 6. Bond Length and the Bond Angle of the Studied Inhibitors (C1, C2, and C3)

	compounds	C1	C2	C3
bond length	C1−C2	1.519	1.519	1.519
	C2−C3	1.519	1.519	1.519
	C4−N5	1.399	1.394	1.402
	N5−C6	1.459	1.456	1.462
	C6−C7	1.520	1.520	1.519
	C8−N9	1.412	1.412	1.409
	N9−N10	1.255	1.256	1.256
	N10−C11	1.418	1.415	1.416
bond angle	C1−C2−C3	114.092	115.181	112.900
	C4−N5−C6−C7	67.733	70.113	66.609
	C8−N9−N10−C11	180	180	180

3.6.2. Frontier Orbital Energies and Global Reactivity Parameters. The highest occupied molecular orbital, abbreviated HOMO, and the lowest unoccupied molecular orbital, abbreviated LUMO, are the two types of boundary molecular orbitals found in molecules (LUMO). Low kinetic stability is associated with molecules with a small HOMO−LUMO gap and high chemical reactivity.[48,49] Applying Koopman's theory led to estimating molecular properties associated with reactivity

https://doi.org/10.1021/acsomega.3c00741
ACS Omega 2023, 8, 21571−21584

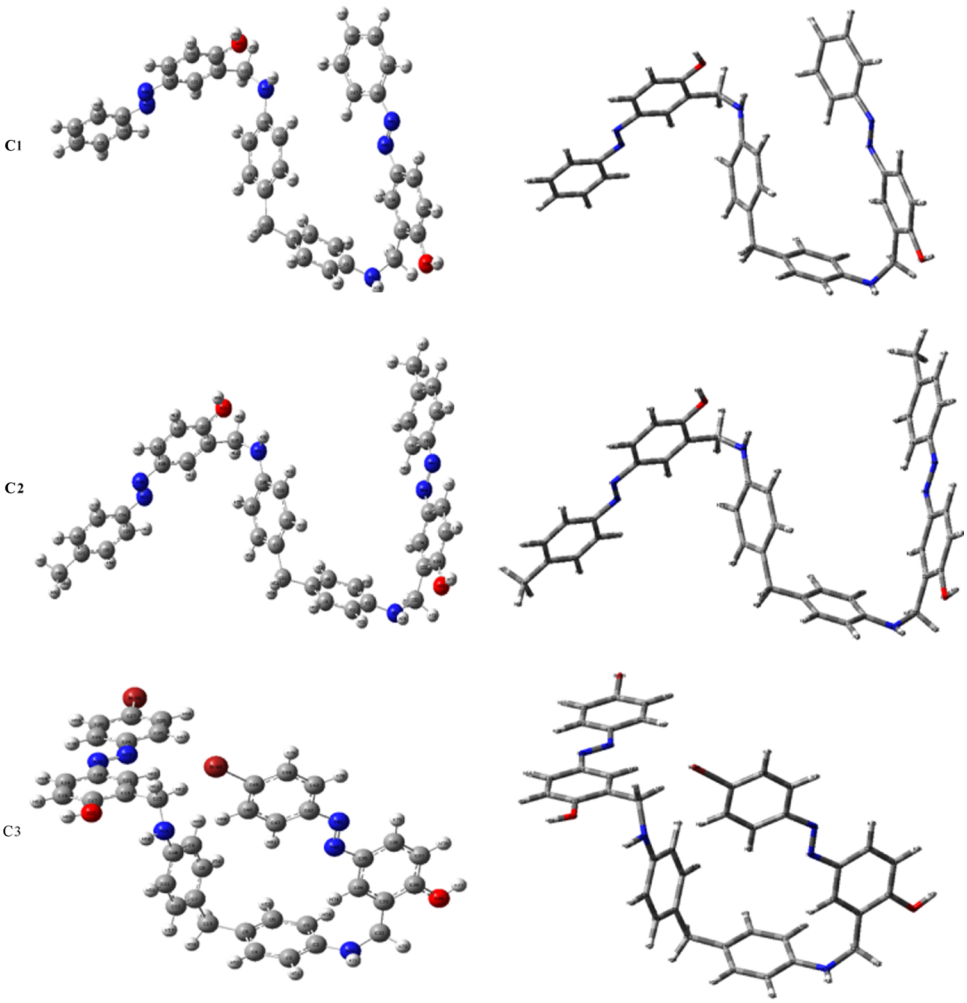

Figure 8. Optimized structure of the three inhibitors (C1, C2, and C3) obtained at the DFT/B3LYP/6-311G (d, p) level.

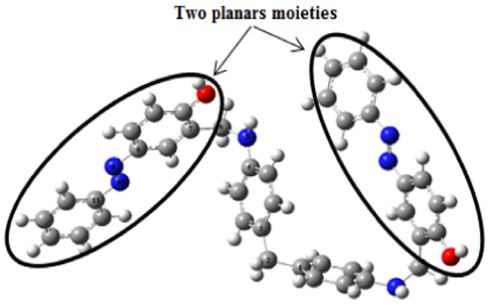

Figure 9. Selected planar moieties of the inhibitors (C1, C2, and C3).

and selectivity based on the DFT-Koopman's theory.[50−52] To get an approximation of the electron affinity (A) and the ionization potential (I), the negative values of (E_{HOMO}) and (E_{LUMO}) are taken, respectively. This is done in quantitative terms.[52] Furthermore, the relationships used in all of these calculations are as follows[53,54]

$$\text{energy band gap: } E_g = E_{LUMO} - E_{HOMO} \quad (11)$$

$$\text{electron Affinity: } A = -E_{LUMO} \quad (12)$$

$$\text{ionization potential: } I = -E_{HOMO} \quad (13)$$

$$\text{chemical hardness: } \eta = \frac{E_{LUMO} - E_{HOMO}}{2} \quad (14)$$

$$\text{chemical softness: } \delta = \frac{1}{2\eta} \quad (15)$$

$$\text{electro} - \text{negativity: } \chi = \frac{-(E_{LUMO} + E_{HOMO})}{2} \quad (16)$$

$$\text{chemical potential: } \mu = \frac{E_{LUMO} + E_{HOMO}}{2} \quad (17)$$

$$\text{global electrophilicity index: } \omega = \frac{\mu^2}{2\eta} \quad (18)$$

$$\text{fraction of electron transferred: } \Delta N = \frac{\chi_{Fe} - \chi_{inh}}{2(\eta_{Fe} + \eta_{inb})} \quad (19)$$

$$\text{molecule} - \text{metal interaction energy: } \Delta\psi = \frac{\chi_{Fe} - \chi_{inh}}{4(\eta_{Fe} + \eta_{inb})} \quad (20)$$

$$\text{energy associated with a backing donation: } E_{b-d} = \frac{-\eta}{4} \quad (21)$$

https://doi.org/10.1021/acsomega.3c00741
ACS Omega 2023, 8, 21571−21584

Table 7. Global Reactivity Descriptors of the Studied Inhibitors According to Density Functional Theory (DFT) (C1, C2, and C3)

comp		E_{HOMO} (eV)	E_{LUMO} (eV)	E_g (eV)	η (eV)	δ (eV^{-1})	χ (eV)	μ (eV)	ω	ΔN	$\Delta\psi$	E_{b-d} (eV)
C_1	[a]	−5.113	−2.308	2.8058	1.403	0.356	3.710	−3.710	4.907	1.1724	0.204	−0.351
	[b]	−4.905	−2.065	2.8393	1.420	0.352	3.485	−3.485	4.278	1.240	0.619	−0.355
C_2	[a]	−4.949	−2.192	2.7568	1.378	0.363	3.571	−3.571	4.625	1.2439	0.216	−0.345
	[b]	−4.737	−1.954	2.7838	1.392	0.359	3.345	−3.345	4.020	2.784	0.656	−0.348
C_3	[a]	−5.184	−2.481	2.7030	1.351	0.370	3.832	−3.832	5.433	1.1720	0.184	−0.338
	[b]	−4.963	−2.223	2.7400	1.370	0.365	3.593	−3.593	4.711	1.240	0.622	−0.342

[a]6-311G (d, p) basis set. [b]6-31G (d, p) basis set.

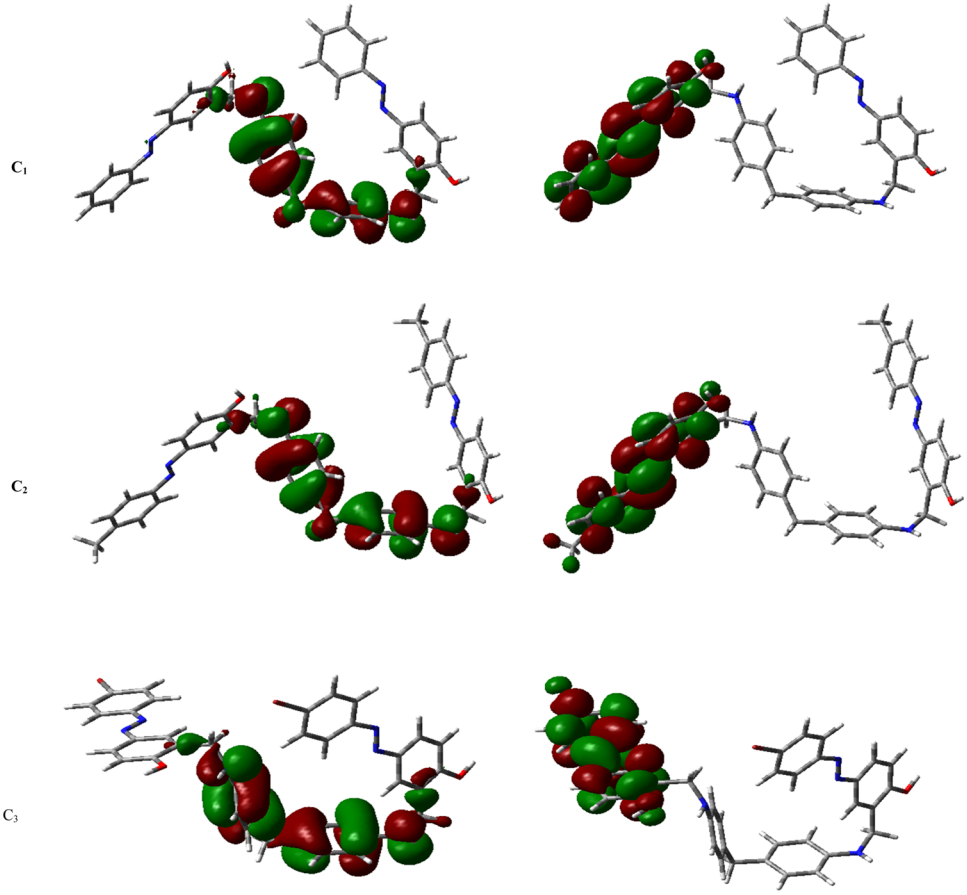

Figure 10. Schematic representation of HOMO and LUMO of inhibitors (C1, C2, and C3) obtained by DFT at the B3LYP/6-311G (d, p) level.

knowing that χ_{Fe}: electronegativity of iron (7.0 eV); χ_{inh}: electronegativity of the inhibitors; η_{Fe}: chemical hardness of iron (0 eV); and η_{inb}: chemical hardness of the inhibitors.

As shown in Table 7, calculations establish that the highest E_{HOMO} is observed in compound C2 (−4.949 eV), which may be attributed to the additional inductive effect (electron-donating) of lateral methyl groups. Inhibitors with a high E_{HOMO} can remarkably push electrons into the low vacancy orbital of the corrosive environment, thereby delaying the anodic processes.[55−57] In addition, the stability of LUMO supports the electron-receiving potential of the corrosion inhibitor, facilitating the interaction between them. This reaction improves the isolation of the corrosive material from the corrosive environment. Further, the lowest E_{LUMO} is observed in compound C3 (−2.481 eV), which may be attributed to the other electron-withdrawing group (i.e., bromo).

The low energy gap has also been associated with molecular ductility, chemical reaction, kinetic instability, and good anticorrosion potential.[58,59] As illustrated in Table 7, the values of E_g are very close and may be classified in the following order: C3 > C2 > C1, indicating that compound C3 would offer adequate anticorrosion protection. Therefore, the inhibitors studied generally have a low energy band, meaning that they can be anticorrosion materials. Also, as depicted in Table 7, all azo compounds' chemical potential values are negative, implying that the azo compounds are stable.

Besides, the low potential value (−3.832 eV) and the significant electrophilicity value (5.433) for compound C3 favor its electrophilic behavior. On the contrary, the high potential value (−3.571 eV) and the low electrophilicity value (4.625) for compound C2 promote its nucleophilic behavior.[60] This is a result that corresponds to the HOMO and LUMO energies values.[61] Some electrons were transferred (ΔN); this parameter is generally used to indicate the ability of a molecule to accept or transfer electrons to or from a metal.[62−65] The inhibitor can donate its electron to the metal if $\Delta N > 0$, and the

https://doi.org/10.1021/acsomega.3c00741
ACS Omega 2023, 8, 21571−21584

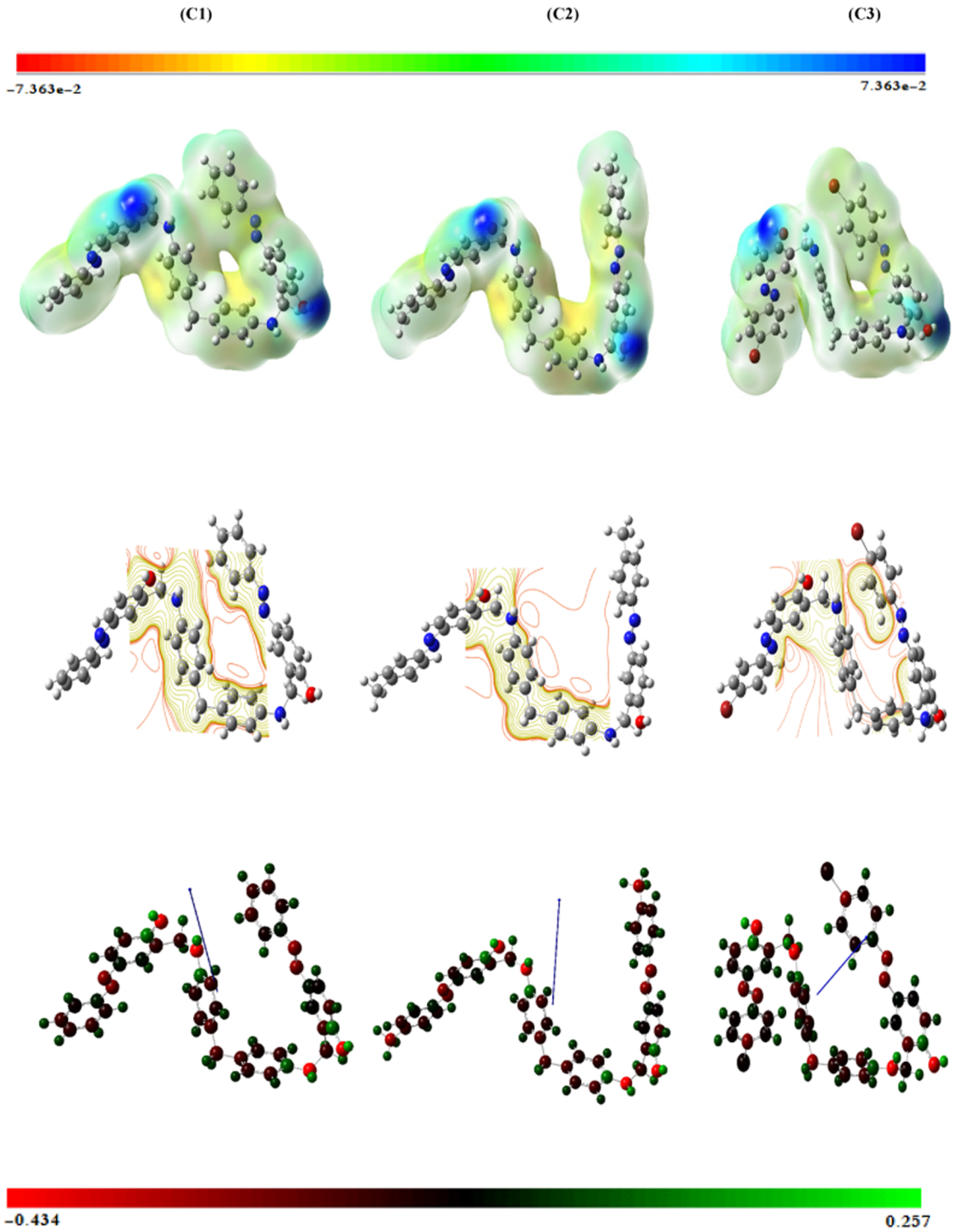

Figure 11. Electrostatic properties of inhibitors (C1, C2, and C3): 3D MEP contour map at the top of the figure and 2D MEP in the middle, and MEP maps for the dipole and the Mullikan charge populations are displayed at the bottom (the region that is rich in electrons appears red, whereas the area that lacks electrons appears blue).

reverse occurs in the case of $\Delta N < 0$. Thus, the positive values of ΔN for all of the inhibitors studied imply that the electron donation is from the inhibitor to the metal surface and follows the order C2 > C1 > C3, along with molecule−metal interaction energy ($\Delta\psi$) that follows the same trend for the presented property of the three molecules. These results are compatible with experimental inhibition efficiency. Moreover, the inverse grant can be obtained from E_{b-d}. Indeed, a negative sign of E_{b-d} indicates that back donation from the metal to the inhibitor is energetically favorable. All of the inhibitors have ∼(−0.34 eV). The back donation and donation processes strengthen the inhibitors' adsorption on the iron surface.

Figure 10 illustrates the HOMO map of C1, C2, and C3 inhibitors. The HOMO map is essentially delocalized over the middle moiety (i.e., two benzene rings attached by the CH_2 group and two primary amino groups −NH−CH_2−), indicating that this part is rich in electrons and is the one that can donate to the metal. Similarly, the LUMO diagram for inhibitors clearly

https://doi.org/10.1021/acsomega.3c00741
ACS Omega 2023, 8, 21571−21584

shows the delocalization of vacant lower molecular orbitals on a single planar moiety of azo compounds (two benzene rings attached by the −N═N− group), except the carbon atom of the lateral methyl group in compound C2. This phenomenon indicates that the LUMO of the inhibitors is available for back donation.

3.6.3. Corrosion Inhibition and the Molecular Electrostatic Potential (MEP). The molecular electrostatic potential, often known as the MEP, is used to predict the reactivity of inhibitor molecules and the overall charge distribution.[66] For all of the researched azo compounds, the color coding for these maps runs from −0.07363 au (dark red) to 0.07363 au (dark blue). The MEP map and contour plot of C1, C2, and C3 were made in the optimal geometry and were carried out using the Gauss 05 view. These results are displayed at the top of the page (Figure 11).

The MEP map, which can be found in Figure 11, makes it abundantly evident that the regions surrounding the hydrogen atoms of the amine group and hydroxyl groups' hydrogen atoms have a significant lack of electrons (blue color).

In addition, there are the hydrogen atoms within the benzene rings, the hydrogen atoms within the two methyl groups that make up the C2 inhibitor, and its binding site for electrophiles. The second presentation of the MEP and 2D contour map (Figure 11) shows that the electron-rich region around all nitrogen, oxygen atoms, and benzene rings are also evident. The space around the two Br atoms for C3 is the electronegative region due to its inductive effect (i.e., charge transfer from the benzene ring to the bromo atoms) and bonding sites to nucleophiles.

As an excellent way to explain the differences in electromagnetism of atoms in a molecule, the charge population and direction of the dipole moment, depicted at the bottom of Figure 1, are often used to support MEP mapping.[62] For example, the hydrogen atoms that make up the amino and hydroxyl groups have the most significant positive charge (green). The MEP map depicts them as having the darkest shade of blue possible.

The Mulliken charge populations and the dipole moment direction are projected onto the molecular plane for the three Schiff bases. The charge population and direction of the dipole moment can be comprehended by examining the electrostatic potential (bottom panels of 1), which identifies electron density-rich regions centered on O atoms in the hydroxyl group, N atoms in the −N═N− group, C atoms of the carbon bone chain, and some carbon atoms in benzene rings. Electrophiles often attack the locations with the highest electron density. Therefore, the active centers are O, N, and C atoms, with the most significant capacity to attach to the metal surface. In contrast, the HOMO (Figure 10) was mainly spread across the atoms, as mentioned earlier. Therefore, these regions are likely the major bonding sites.[63,64]

4. CONCLUSIONS

This work was dedicated to investigating the inhibitory activity of three prepared azo compounds derived from Schiff bases, namely, bis[5-(phenylazo)-2-hydroxybenzaldehyde]-4,4′-diaminophenylmethane (C1), bis[5-(4-methylphenylazo)-2-hydroxybenzaldehyde]-4,4′-diaminophenylmethane (C2), and bis[5-(4-bromophenylazo)-2-hydroxybenzaldehyde]-4,4′-diaminophenylmethane (C3), against corrosion of steel type XC70 in (HCl, 1 M DMSO) medium experimentally using electrochemical measurements and theoretically using density functional theory (DFT). From this research, the main conclusions drawn are listed below:

- Derivatives of Schiff bases azo amines C1, C2, and C3 act as corrosion inhibitors for mild steel type XC70 in solution (HCl, 1 M DMSO). Efficiency increases by increasing concentration. The maximum inhibition efficiency was also observed around C1, i.e., 64.37%; C2, i.e., 87.27%; and C3, i.e., 55.47% at the concentration (6×10^{-5} M) at ambient temperature.
- The corrosion rate of XC70 decreases with mounting concentrations of C1, C2, and C3.
- Inhibitors C1, C2, and C3 act as mixed but mainly anodic inhibitors, i.e., they inhibit cathodic and anodic reactions during corrosion.
- The Langmuir adsorption isotherm is the best way to describe the inhibitors' adsorption (XC70).
- These values were found to be −42.58, −43.29, and −40.92 kJ/mol for compounds C1, C2, and C3, respectively, indicating that the adsorption of the inhibitors onto the metal surface was a spontaneous reaction.
- The predominant adsorption of the C1, C2, and C3 inhibitors on extrusive steel XC70 is chemical.
- The order of inhibitors in terms of efficacy is C2 > C1 > C3.
- The theoretical calculations are in good agreement with the experimental results, where (ΔN) and ($\Delta\psi$) obey the following order: C2 > C1 > C3.

- Compound C2 favors its nucleophilic character because of the trend of HOMO energy: C2 > C1 > C3, which may be attributed to an inductive effect (electron-donating) of lateral methyl groups. On the contrary, compound C3 favors its electrophilic character, which may be attributed to electron-withdrawing groups (bromo), which do decrease the LUMO energy. Therefore, this compound has the most significant value of the back-donation energy (E_{b-d}).
- The negative sign of (E_{b-d}) indicates that back donation to the inhibitor is energetically favorable.
- The molecular electrostatic potential (MEP) and Mulliken charge populations indicate that inhibitors adsorb through the N and O atoms and π-electron active centers.
- The theoretical calculations and experimental findings concur that three were produced.

AUTHOR INFORMATION

Corresponding Author

Noureddine Elboughdiri − *Chemical Engineering Department, College of Engineering, University of Ha'il, Ha'il 81441, Saudi Arabia; Chemical Engineering Process Department, National School of Engineers Gabes, University of Gabes, Gabes 6029, Tunisia;* orcid.org/0000-0003-2923-3062; Email: ghilaninouri@yahoo.fr

Authors

Ammar Zobeidi − *Department of Chemistry, Faculty of Exact Sciences, University of El Oued, El Oued 39000, Algeria; Pollution & Waste Treatment Laboratory (PWTL), University of Ouargla, Ouargla 30000, Algeria*

Salah Neghmouche Nacer − *Department of Chemistry, Faculty of Exact Sciences, University of El Oued, El Oued 39000, Algeria*

https://doi.org/10.1021/acsomega.3c00741
ACS Omega 2023, 8, 21571−21584

Salem Atia − *Pollution & Waste Treatment Laboratory (PWTL), University of Ouargla, Ouargla 30000, Algeria*
Latifa Kribaa − *Pollution & Waste Treatment Laboratory (PWTL), University of Ouargla, Ouargla 30000, Algeria*
Aicha Kerassa − *Laboratory Valorization and Technology of Saharan Resources (VTRS), University of El-Oued, El-Oued 39000, Algeria*
Abasse Kamarchou − *Pollution & Waste Treatment Laboratory (PWTL), University of Ouargla, Ouargla 30000, Algeria*
Mousa AlNoaimi − *Chemistry Department, Faculty of Science, Kuwait University, Safat 13060, Kuwait; Department of Chemistry, Faculty of Sciences, The Hashemite University, Zarqa 13133, Jordan*
Djamel Ghernaout − *Chemical Engineering Department, College of Engineering, University of Ha'il, Ha'il 81441, Saudi Arabia; Chemical Engineering Department, Faculty of Engineering, University of Blida, Blida 09000, Algeria;* orcid.org/0000-0002-0806-3810
Mohamed A. Ali − *School of Biotechnology, Badr University in Cairo (BUC), Badr, Cairo 11829, Egypt*
Abdelmajeed Adam Lagum − *Department of Civil Engineering, Faculty of Engineering, Isra University, Amman 11622, Jordan*

Complete contact information is available at: https://pubs.acs.org/10.1021/acsomega.3c00741

Author Contributions

The manuscript was written through contributions of all authors. All authors have given approval to the final version of the manuscript.

Notes

The authors declare no competing financial interest.

■ ACKNOWLEDGMENTS

The authors are highly thankful to the Algerian General Directorate for Scientific Research and Technological Development, and the authors of this piece would like to express their gratitude to the Pollution & Waste Treatment Laboratory (PWTL) at the University of Ouargla, Algeria.

■ REFERENCES

(1) Chebabe, D.; Abbout, S.; Damej, M.; Oubair, A.; Lakbaibi, Z.; Dermaj, A.; Benassaoui, H.; Doubi, M.; Hajjaji, N. Electrochemical and theoretical study of corrosion inhibition on carbon steel in 1M HCl medium by 1,10-bis(4-amino-3-methyl-1,2,4-triazole-5-thioyl) decane. *J. Fail. Anal. Prev.* **2020**, *20*, 1673−1683.
(2) Winkler, D. A. Predicting the performance of organic corrosion inhibitors. *Metals* **2017**, *7*, 553.
(3) Chadwick, D.; Hashemi, T. Electron spectroscopy of corrosion inhibitors: Surface Films formed by 2-mercaptobenzothiazole and 2-mercaptobenzimidazole on copper. *Surf. Sci.* **1979**, *89*, 649−659.
(4) Cruz, J.; Martínez, R.; Genesca, J.; García-Ochoa, E. Experimental and theoretical study of 1-(2-ethylamino)-2-methylimidazoline as an inhibitor of carbon steel corrosion in acid media. *J. Electroanal. Chem.* **2004**, *566*, 111−121.
(5) Migahed, M. A. Electrochemical investigation of the corrosion behaviour of mild steel in 2M HCl solution in presence of 1-dodecyl-4-methoxy pyridinium bromide. *Mater. Chem. Phys.* **2005**, *93*, 48−53.
(6) Ismail, K. M. Evaluation of cysteine as environmentally friendly corrosion inhibitor for copper in neutral and acidic chloride solutions. *Electrochim. Acta* **2007**, *52*, 7811−7819.
(7) Atia, S.; Boudehane, A.; Zobeidi, A.; Douadi, T.; Lounas, A.; Al-Noaimi, M.; Gherraf, N. Cyclic Voltammetry Studies of Synthesized New Azo Schiff bases. *Res. J. Pharm. Biol. Chem. Sci.* **2017**, *8*, 840−847.
(8) Soltani, N.; Behpour, M.; Ghoreishi, S. M.; Naeimi, H. Corrosion inhibition of mild steel in hydrochloric acid solution by some double Schiff bases. *Corros. Sci.* **2010**, *52*, 1351−1361.
(9) Calderón, J.; Vásquez, F. A.; Carreño, J. A. Adsorption and performance of the 2-mercaptobenzimidazole as a carbon steel corrosion inhibitor in EDTA solutions. *Chem. Phys.* **2017**, *185*, 218−226.
(10) Sadeghi Erami, R.; Amirnasr, M.; Meghdadi, S.; Talebian, M.; Farrokhpour, H.; Raeissi, K. Carboxamide derivatives as new corrosion inhibitors for mild steel protection in hydrochloric acid solution. *Corros. Sci.* **2019**, *151*, 190−197.
(11) Sarkar, S.; Sengupta, S.; Saha, S. K.; Murmu, N. C.; Dutta, S.; Banerjee, P. Quantifying corrosion inhibition on mild steel surface using run length statistics-based texture analysis. *J. Adhes. Sci. Technol.* **2022**, *36*, 2505−2526.
(12) Abdeslam, A.; Mounir, M.; Mohamed, Z.; Zouhair, L.; Mohamed, A. Experimental and theoretical study on corrosion inhibition of new synthesized menthone derivatives (menthopyrazole compounds) for mild steel in 1M HCl solution. *Mediterr. J. Chem.* **2020**, *10*, 62−76.
(13) Haris, N. I. N.; Sobri, S.; Yusof, Y. A.; Kassim, N. K. An overview of molecular dynamic simulation for corrosion inhibition of ferrous metals. *Metals* **2021**, *11*, No. 46.
(14) Nabatipour, S.; Mohammadi, S.; Mohammadi, A. Synthesis and comparison of two chromone based Schiff bases containing methoxy and acetamido substitutes as highly sustainable corrosion inhibitors for steel in hydrochloric acid. *J. Mol. Struct.* **2020**, *1217*, No. 128367.
(15) El-khlifi, A.; Saadouni, M.; Ijoub, R.; Oubihi, A.; Elaoufir, Y.; Boukhriss, S.; Ouhssine, M. Synthesis and corrosion inhibition of mild steel in a phosphoric acid solution of a novel benzothiazine derivative. *Port. Electrochim. Acta* **2022**, *39*, 33−46.
(16) El Assyry, A.; Benali, B.; Lakhrissi, B.; El Faydy, M.; Ebn Touhami, M.; Touir, R.; Touil, M. Experimental and theoretical comparatives investigation of mild steel corrosion inhibition by quinoxalinone derivatives in 1M HCl. *Res. Chem. Intermed.* **2015**, *41*, 3419−3431.
(17) Benabid, S.; Douadi, T.; Issaadi, S.; Penverne, C.; Chafaa, S. Electrochemical and DFT studies of a new synthesized Schiff base as corrosion inhibitor in 1M HCl. *Measurement* **2017**, *99*, 53−63.
(18) Kribaa, L.; Atia, S.; Boudehane, A.; Bader, R. M. M.; Gherraf, N. Synthesis, characterization and antioxidant activity studies of new azo-compounds. *J. Biochem. Technol.* **2019**, *10*, 85.
(19) Atia, S.; Douadi, T.; Douadi, A.; Lanez, T.; Al-Noaimi, M. Synthesis, spectroscopic studies of new azo ligands Schiff base and amines derived of 5-phenylazo-2-hydroxybenzaldehyde. *J. Chem. Pharm. Res.* **2015**, *7*, 692−696.
(20) Ziouani, A.; Atia, S.; Hamani, H.; Douadi, T.; Al-Noaimi, M.; Gherraf, N. Molecular dynamic simulation and experimental investigation on the synergistic mechanism and synergistic effect of (1Z) N [2 (Methylthio) phenyl] 2oxopropanehydrazonoyl chloride (s1) corrosion inhibitor on mild steel in acid medium 1M HCl. *J. Indian Chem. Soc.* **2023**, *100*, No. 100832.
(21) Behpour, M.; Mohammadi, N.; Alian, E. Electrochemical and mass loss investigations of new schiff base as corrosion inhibitor for mild steel. *J. Iron Steel Res. Int.* **2014**, *21*, 121−124.
(22) Suhasaria, A.; Murmu, M.; Satpati, S.; Banerjee, P.; Sukul, D. Bis-benzothiazoles as efficient corrosion inhibitors for mild steel in aqueous HCl: Molecular structure-reactivity correlation study. *J. Mol. Liq.* **2020**, *313*, No. 113537.
(23) Djenane, M.; Chafaa, S.; Chafai, N.; Kerkour, R.; Hellal, A. Synthesis, spectral properties and corrosion inhibition efficiency of new ethyl hydrogen [(methoxyphenyl) (methylamino) methyl] phosphonate derivatives: Experimental and theoretical investigation. *J. Mol. Struct.* **2019**, *1175*, 398−413.
(24) Hariharan, P. C.; Pople, J. A. The influence of polarization functions on molecular orbital hydrogenation energies. *Theor. Chim. Acta.* **1973**, *28*, 213−222.
(25) Christenholz, C. L.; Obenchain, D. A.; Peebles, R. A.; Peebles, S. A. Rotational spectroscopic studies of C−H···F interactions in the vinyl

fluoride···difluoromethane complex. *J. Phys. Chem. A* **2014**, *118*, 1610−1616.
(26) Bahrami, M. J.; Hosseini, S. M. A.; Pilvar, P. Experimental and theoretical investigation of organic compounds as inhibitors for mild steel corrosion in sulfuric acid medium. *Corros. Sci.* **2010**, *52*, 2793−2803.
(27) Rajeswari, V.; Kesavan, D.; Gopiraman, M.; Viswanathamurthi, P. Inhibition of cast iron corrosion in acid, base, and Neutral Media using Schiff base derivatives. *J Surfactants Deterg.* **2013**, *16*, 571−580.
(28) Hosseini, S. M. A.; Azimi, A. The inhibition of mild steel corrosion in acidic medium by 1-methyl-3-pyridin-2-yl-thiourea. *Corros. Sci.* **2009**, *51*, 728−732.
(29) Fawzy, A.; Toghan, A. Inhibition evaluation of chromotrope dyes for the corrosion of mild steel in an acidic environment: Thermodynamic and kinetic aspects. *ACS Omega* **2021**, *6*, 4051−4061.
(30) Ashassi-Sorkhabi, H.; Shabani, B.; Aligholipour, B.; Seifzadeh, D. The effect of some Schiff bases on the corrosion of aluminum in hydrochloric acid solution. *Appl. Surf. Sci.* **2006**, *252*, 4039−4047.
(31) Kaya, S.; Erkan, S.; Şimşek, S.; Kumar, A. Ionic liquids as corrosion inhibitors. *ACS Symp. Ser.* **2021**, 103−119.
(32) Attabi, S.; Mokhtari, M.; Taibi, Y.; Abdel-Rahman, I.; Hafez, B.; Elmsellem, H. Electrochemical and tribological behavior of surface-treated titanium alloy ti−6al−4v. *J. Bio- Tribo-Corros.* **2018**, No. 2.
(33) Fekry, A. M.; Ameer, M. A. Corrosion inhibition of mild steel in acidic media using newly synthesized heterocyclic organic molecules. *Int. J. Hydrogen Energy* **2010**, *35*, 7641−7651.
(34) Emregül, K. C.; Düzgün, E.; Atakol, O. The application of some polydentate Schiff base compounds containing aminic nitrogens as corrosion inhibitors for mild steel in acidic media. *Corros. Sci.* **2006**, *48*, 3243−3260.
(35) Khaled, K. F.; Babić-Samardžija, K.; Hackerman, N. Theoretical study of the structural effects of polymethylene amines on corrosion inhibition of iron in acid solutions. *Electrochim. Acta.* **2005**, *50*, 2515−2520.
(36) Stoynov, Z. Impedance modelling and data processing: Structural and Parametrical estimation. *Electrochim. Acta.* **1990**, *35*, 1493−1499.
(37) Bredar, A. R. C.; Chown, A. L.; Burton, A. R.; Farnum, B. H. Electrochemical impedance spectroscopy of metal oxide electrodes for energy applications. *ACS Appl. Energy Mater.* **2020**, *3*, 66−98.
(38) Kallay, N.; Preočanin, T.; Kovačević, D.; Lützenkirchen, J.; Villalobos, M. Thermodynamics of the reactions at solid/liquid interfaces. *Croat. Chem. Acta.* **2011**, *84*, 1−10.
(39) Chakib, I.; Elmsellem, H.; Sebbar, N.; Lahmidi, S.; Nadeem, A.; Essassi, E.; Ouzidan, Y.; Abdel-Rahman, I.; Bentiss, F.; Hammouti, B. Electrochemical, gravimetric and theoretical evaluation of (4Z)-2, 5-dimethyl-4-(4-methylpyrimido [1, 2-a] benzimidazol-2 (1H)-ylidene)-2, 4-dihydro-3H-pyrazol-3-one (P1) as a corrosion inhibitor for mild steel in 1 M HCl solution. *J. Mater. Environ. Sci* **2016**, *7*, 1866−1881.
(40) Chkirate, K.; Azgaou, K.; Elmsellem, H.; El Ibrahimi, B.; Sebbar, N. K.; Anouar, E. H.; Benmessaoud, M.; El Hajjaji, S.; Essassi, E. M. Corrosion inhibition potential of 2-[(5-methylpyrazol-3-yl) methyl] benzimidazole against carbon steel corrosion in 1M HCl solution: Combining experimental and theoretical studies. *J. Mol. Liq.* **2021**, *321*, No. 114750.
(41) Karthik, G.; Sundaravadivelu, M. Studies on the inhibition of mild steel corrosion in hydrochloric acid solution by Atenolol Drug. *Egypt. J. Pet.* **2016**, *25*, 183−191.
(42) Touhami, F.; Aouniti, A.; Abed, Y.; Hammouti, B.; Kertit, S.; Ramdani, A.; Elkacemi, K. Corrosion inhibition of Armco iron in 1M HCl Media by new bipyrazolic derivatives. *Corros. Sci.* **2000**, *42*, 929−940.
(43) Hong, T.; Sun, Y. H.; Jepson, W. P. Study on corrosion inhibitor in large pipelines under multiphase flow using EIS. *Corros. Sci.* **2002**, *44*, 101−112.
(44) Mabrouk, S.; Bebba, A. A.; Kamarchou, A.; Zobeidi, A. Adsorption capacity of pollutants by using local clay mineral from urban wastewater Touggourt (south-east Algeria). *Asian J. Res. Chem. Pharm. Sci.* **2020**, *13*, 85−90.
(45) Mittal, K. L. *Contact Angle, Wettability and Adhesion*; CRC Press, an imprint of Taylor & Francis, 2003.
(46) Behpour, M.; Ghoreishi, S. M.; Mohammadi, N.; Soltani, N.; Salavati-Niasari, M. Investigation of some Schiff base compounds containing disulfide bond as HCl corrosion inhibitors for mild steel. *Corros. Sci.* **2010**, *52*, 4046−4057.
(47) Daoud, D.; Douadi, T.; Hamani, H.; Chafaa, S.; Al-Noaimi, M. Corrosion inhibition of mild steel by two new S-heterocyclic compounds in 1M HCl: Experimental and computational study. *Corros. Sci.* **2015**, *94*, 21−37.
(48) Abd El-Lateef, H. M. Experimental and computational investigation on the corrosion inhibition characteristics of mild steel by some novel synthesized imines in hydrochloric acid solutions. *Corros. Sci.* **2015**, *92*, 104−117.
(49) Koparir, P.; Omer, R.; Karatepe, M.; Ahmed, L. Synthesis, characterization, and theoretical inhibitor study for (1e,1′e)-2,2′-thiobis(1-(3-mesityl-3-methylcyclobutyl) ethan-1-one) dioxime. *ECJSE* **2021**, *8*, 1495−1510.
(50) Yin, D.; Yang, L.; Tan, B.; Ma, T.; Zhang, S.; Wang, Y.; Guo, L.; Gao, B.; He, Y. Theoretical and electrochemical analysis on inhibition effects of benzotriazole derivatives (UN- and methyl) on copper surface. *J. Mol. Struct.* **2021**, *1243*, No. 130871.
(51) Fleming, J. *Frontier Orbitals and Organic Chemical Reactions*, 1st ed.; John Wiley & Sons: London, 1976.
(52) Pearson, R. G. Hard and soft acids and bases. *J. Am. Chem. Soc.* **1963**, *85*, 3533−3539.
(53) Dewar, M. J. S.; Thiel, W. Ground states of molecules. 38. the MNDO method. approximations and parameters. *J. Am. Chem. Soc.* **1977**, *99*, 4899−4907.
(54) Parr, R. G.; Pearson, R. G. Absolute hardness: Companion parameter to absolute electronegativity. *J. Am. Chem. Soc.* **1983**, *105*, 7512−7516.
(55) Moseev, T. D.; Varaksin, M. V.; Virlova, E. A.; Medvedeva, M. V.; Svalova, T. S.; Melekhin, V. V.; Tsmokaluk, A. N.; Kozitsina, A. N.; Charushin, V. N.; Chupakhin, O. N. Fluoroaromatic 2h-imidazole-based push-pull fluorophores: Synthesis, theoretical studies, and application opportunities as probes for sensing the ph in Saliva. *Dyes Pigm.* **2022**, *202*, No. 110251.
(56) Guo, L.; Ren, X.; Zhou, Y.; Xu, S.; Gong, Y.; Zhang, S. Theoretical evaluation of the corrosion inhibition performance of 1,3-thiazole and its amino derivatives. *Arab. J. Chem.* **2017**, *10*, 121−130.
(57) Saha, S. K.; Ghosh, P.; Hens, A.; Murmu, N. C.; Banerjee, P. Density functional theory and molecular dynamics simulation study on corrosion inhibition performance of mild steel by Mercapto-quinoline Schiff base corrosion inhibitor. *Phys. E* **2015**, *66*, 332−341.
(58) Hu, J.; Zeng, D.; Zhang, Z.; Shi, T.; Song, G.-L.; Guo, X. 2-hydroxy-4-methoxy-acetophenone as an environment-friendly corrosion inhibitor for AZ91D magnesium alloy. *Corros. Sci.* **2013**, *74*, 35−43.
(59) Rbaa, M.; Lakhrissi, B. Novel oxazole and imidazole based on 8-hydroxyquinoline as a corrosion inhibition of mild steel in HCl solution: Insights from experimental and computational studies. *Surf. Interfaces* **2019**, *15*, 43−59.
(60) Sharma, K.; Melavanki, R.; Patil, S. S.; Kusanur, R.; Patil, N. R.; Shelar, V. M. Spectroscopic behavior, FMO, NLO and NBO analysis of two novel aryl boronic acid derivatives: Experimental and Theoretical Insights. *J. Mol. Struct.* **2019**, *1181*, 474−487.
(61) Singh, R. N.; Kumar, A.; Tiwari, R. K.; Rawat, P.; Gupta, V. P. A combined experimental and Quantum Chemical (DFT and aim) study on molecular structure, spectroscopic properties, NBO and Multiple Interaction Analysis in a novel ethyl 4-[2-(carbamoyl) hydrazinylidene]-3,5-dimethyl-1h-pyrrole-2-carboxylate and its dimer. *J. Mol. Struct.* **2013**, *1035*, 427−440.
(62) Kerassa, A.; Belaidi, S.; Harkati, D.; Lanez, T.; Prasad, O.; Sinha, L. Investigations on molecular structure, electronic properties, NLO properties and comparison of drug-likeness of triazolothiadiazole derivatives by quantum methods and QSAR analysis. *Rev. Theor. Sci.* **2016**, *4*, 85−96.

https://doi.org/10.1021/acsomega.3c00741
ACS Omega 2023, 8, 21571−21584

(63) Roque, J. M.; Pandiyan, T.; Cruz, J.; García-Ochoa, E. DFT and electrochemical studies of Tris(benzimidazole-2-ylmethyl) amine as an efficient corrosion inhibitor for carbon steel surface. *Corros. Sci.* **2008**, *50*, 614−624.
(64) Obot, I. B.; Macdonald, D. D.; Gasem, Z. M. Density functional theory (DFT) as a powerful tool for designing new organic corrosion inhibitors. part 1: An overview. *Corros. Sci.* **2015**, *99*, 1−30.
(65) Lashkari, M.; Arshadi, M. R. DFT studies of pyridine corrosion inhibitors in electrical double layer: Solvent, substrate, and electric field effects. *Chem. Phys.* **2004**, *299*, 131−137.
(66) Nourpour, P.; Hamdi, M.; Taghipour, S.; Vafaee, M.; Heydarzadeh, A. Theoretical evaluation of spirocyclic compounds asgreencorrosion inhibitors for Carbon Steel. *Thin Solid Films* **2023**, *766*, No. 139658.

https://doi.org/10.1021/acsomega.3c00741
ACS Omega 2023, 8, 21571−21584